Regularized Kelvinlet Functions to Model Linear Elasticity for Image-to-Physical Registration of the Breast

Morgan Ringel[1(✉)], Jon Heiselman[1,2], Winona Richey[1], Ingrid Meszoely[3], and Michael Miga[1]

[1] Department of Biomedical Engineering, Vanderbilt University, Nashville, TN, USA
morgan.j.ringel@Vanderbilt.edu
[2] Department of Surgery, Memorial Sloan-Kettering Cancer Center, New York, NY, USA
[3] Division of Surgical Oncology, Vanderbilt University Medical Center, Nashville, TN, USA

Abstract. Image-guided surgery requires fast and accurate registration to align preoperative imaging and surgical spaces. The breast undergoes large nonrigid deformations during surgery, compromising the use of imaging data for intraoperative tumor localization. Rigid registration fails to account for nonrigid soft tissue deformations, and biomechanical modeling approaches like finite element simulations can be cumbersome in implementation and computation. We introduce regularized Kelvinlet functions, which are closed-form smoothed solutions to the partial differential equations for linear elasticity, to model breast deformations. We derive and present analytical equations to represent nonrigid point-based translation ("grab") and rotation ("twist") deformations embedded within an infinite elastic domain. Computing a displacement field using this method does not require mesh discretization or large matrix assembly and inversion conventionally associated with finite element or mesh-free methods. We solve for the optimal superposition of regularized Kelvinlet functions that achieves registration of the medical image to simulated intraoperative geometric point data of the breast. We present registration performance results using a dataset of supine MR breast imaging from healthy volunteers mimicking surgical deformations with 237 individual targets from 11 breasts. We include analysis on the method's sensitivity to regularized Kelvinlet function hyperparameters. To demonstrate application, we perform registration on a breast cancer patient case with a segmented tumor and compare performance to other image-to-physical and image-to-image registration methods. We show comparable accuracy to a previously proposed image-to-physical registration method with improved computation time, making regularized Kelvinlet functions an attractive approach for image-to-physical registration problems.

Keywords: Deformation · registration · elasticity · image-guidance · breast · finite element · Kelvinlet

H. Greenspan et al. (Eds.): MICCAI 2023, LNCS 14228, pp. 344–353, 2023.
https://doi.org/10.1007/978-3-031-43996-4_33

1 Introduction

Image-to-physical registration is a necessary process for computer-assisted surgery to align preoperative imaging to the intraoperative physical space of the patient to in-form surgical decision making. Most intraoperatively utilized image-to-physical regis-trations are rigid transformations calculated using fiducial landmarks [1]. However, with better computational resources and more advanced surgical field monitoring sensors, nonrigid registration techniques have been proposed [2, 3]. This has made image-guided surgery more tractable for soft tissue organ systems like the liver, prostate, and breast [4–6]. This work focuses specifically on nonrigid breast registration, although these methods could be adapted for other soft tissue organs. Current guidance technologies for breast conserving surgery localize a single tumor-implanted seed without providing spatial information about the tumor boundary. As a result, resections can have several centimeters of tissue beyond the cancer margin. Despite seed information and large resections, reoperation rates are still high (~17%) emphasizing the need for additional guidance technologies such as computer-assisted surgery systems with nonrigid registration [7].

Intraoperative data available for registration is often sparse and subject to data collection noise. Image-to-physical registration methods that accurately model an elastic soft-tissue environment while also complying with intraoperative data constraints is an active field of research. Determining correspondences between imaging space and geometric data is required for image-to-physical registration, but it is often an inexact and ill-posed problem. Establishing point cloud correspondences using machine learning has been demonstrated on liver and prostate datasets [8, 9]. Deep learning image registration methods like VoxelMorph have also been used for this purpose [10]. However, these methods require extensive training data and may struggle with generalizability. Other non-learning image-to-physical registration strategies include [11] which utilized a corotational linear-elastic finite element method (FEM) combined with an iterative closest point algorithm. Similarly, the registration method introduced in [12] iteratively updated the image-to-physical correspondence between surface point clouds while solving for an optimal deformation state.

In addition to a correspondence algorithm, a technique for modeling a deformation field is required. Both [11] and [12] leverage FEM, which uses a 3D mesh to solve for unique deformation solutions. However, large deformations can cause mesh distortions with the need for remeshing. Mesh-free methods have been introduced to circumvent this limitation. The element-free Galerkin method is a mesh-free method that requires only nodal point data and uses a moving least-squares approximation to solve for a solution [13]. Other mesh-free methods are reviewed in [14]. Although these methods do not require a 3D mesh, solving for a solution can be costly and boundary condition designation is often unintuitive. Having identified these same shortcomings, [15] proposed regularized Kelvinlet functions for volumetric digital sculpting in computer animation applications. This sculpting approach provided de-formations consistent with linear elasticity without large computational overhead.

In this work, we propose an image-to-physical registration method that uses regularized Kelvinlet functions as a novel deformation basis for nonrigid registration. Regularized Kelvinlet functions are analytical solutions to the equations for linear elasticity that we superpose to compute a nonrigid deformation field nearly instantaneously [15].

We utilize "grab" and "twist" regularized Kelvinlet functions with a linearized iterative reconstruction approach (adapted from [12]) that is well-suited for sparse data registration problems. Sensitivity to regularized Kelvinlet function hyperparameters is explored on a supine MR breast imaging dataset. Finally, our approach is validated on an exemplar breast cancer case with a segmented tumor by comparing performance to previously proposed registration methods.

2 Methods

In this section, closed-form solutions to linear elastic deformation responses in an infinite medium are derived to obtain regularized Kelvinlet functions. Then, methods for constructing a superposed regularized Kelvinlet function deformation basis for achieving registration within an iterative reconstructive framework are discussed. Equation notation is written such that constants are italicized, vectors are bolded, and matrices are double-struck letters.

2.1 Regularized Kelvinlet Functions

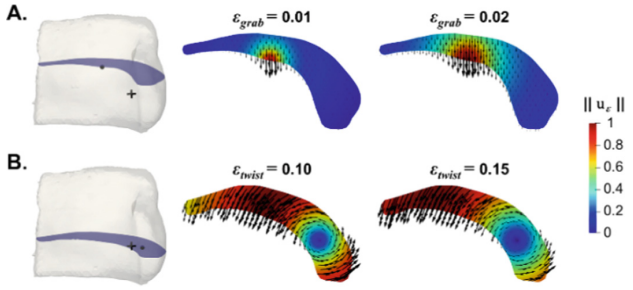

Fig. 1. Visualization of (A) "grab" and (B) "twist" regularized Kelvinlet functions on 2D breast geometry ipsilateral slices at various ε values. (+) denotes nipple location, $(\cdot)$ denotes $\boldsymbol{x_0}$ location.

Linear elasticity in a homogeneous, isotropic media is governed by the Navier-Cauchy equations in Eq. (1), where E is Young's modulus, ν is Poisson's ratio, $\mathbf{u}(\boldsymbol{x})$ is the displacement vector, and $\mathbf{F}(\boldsymbol{x})$ is the forcing function. Analytical displacement solutions to Eq. (1) that represent elastostatic states in an infinite solid can be found for specific forcing functions $\mathbf{F}(\boldsymbol{x})$. Equation (2) represents the forcing function for a point source $\mathbf{F}_\delta(\boldsymbol{x})$, where $\boldsymbol{f}$ is the point source forcing vector and $\boldsymbol{x_0}$ is the load location. The closed-form displacement solution for Eq. (1) given the forcing function in Eq. (2) is classically known as the Kelvin state in Eq. (3), rewritten as a function of $\boldsymbol{r}$ where $\boldsymbol{r} = \boldsymbol{x} - \boldsymbol{x}_0$ and $r = \|\boldsymbol{r}\|$. The coefficients are $a = \frac{(1+\nu)}{2\pi E}$, $b = \frac{a}{[4(1-\nu)]}$, and $\mathbb{I}$ is the identity matrix.

We note that the deformation response is linear with respect to $\boldsymbol{f}$, which implies that forcing functions can be linearly superposed. However, practical use of Eq. (3)

becomes numerically problematic in discretized problems because the displacement and displacement gradient become indefinite as $\boldsymbol{x}$ approaches $\boldsymbol{x_0}$.

$$\frac{E}{2(1+\nu)}\nabla^2 u(x) + \frac{E}{2(1+\nu)(1-2\nu)}\nabla(\nabla \cdot \mathbf{u}(\boldsymbol{x})) + F(x) = 0 \tag{1}$$

$$\mathbf{F_\delta}(x) = f\delta(x - \boldsymbol{x}_0) \tag{2}$$

$$u(\boldsymbol{r}) = \left[\frac{a-b}{r}\mathbb{I} + \frac{b}{r^3}\boldsymbol{r}\boldsymbol{r}^t\right]f = K(r)f \tag{3}$$

To address numerical singularity, regularization is incorporated with a new forcing function Eq. (4), where $r_\varepsilon = \sqrt{r^2 + \varepsilon^2}$ is the regularized distance, and ε is the regularization radial scale. Solving Eq. (1) using Eq. (4) yields a formula for the first type of regularized Kelvinlet functions used in this work in Eq. (5), which is the closed-form, analytical solution for linear elastic translational ("grab") deformations.

$$\mathbf{F}_{\boldsymbol{\varepsilon}}(x) = f\left[\frac{15\varepsilon^4}{8\pi}\frac{1}{r_\varepsilon^7}\right] \tag{4}$$

$$\mathbf{u}_{\boldsymbol{\varepsilon},\mathbf{grab}}(\boldsymbol{r}) = \left[\frac{a-b}{r_\varepsilon}\mathbb{I} + \frac{b}{r_\varepsilon^3}\boldsymbol{r}\boldsymbol{r}^t + \frac{a}{2}\frac{\varepsilon^2}{r_\varepsilon^3}\mathbb{I}\right]f = \mathbb{K}_{\text{grab}}(r)f \tag{5}$$

The second type of regularized Kelvinlet functions represent "twist" deformations which are derived by expanding the previous formulation to accommodate locally affine loads instead of displacement point sources. This is accomplished by associating each component of the forcing function Eq. (4) with the directional derivative of each basis $\boldsymbol{g}_i$ of the affine transformation, leading to the regularized forcing matrix in Eq. (6). An affine loading configuration consisting of pure rotational ("twist") deformation constrains $\mathbb{F}_\varepsilon^{ij}(\boldsymbol{x})$ to a skew-symmetric matrix that simplifies the forcing function to a cross product about a twisting force vector $\boldsymbol{f}$ in Eq. (7). The pure twist displacement field response $\mathbf{u}_{\boldsymbol{\varepsilon},\mathbf{twist}}(\boldsymbol{r})$ to the forcing matrix in Eq. (7) can be represented as the second type of regularized Kelvinlet functions used in this work in Eq. (8).

Superpositions of Eq. (5) and Eq. (8) are used in a registration workflow to model linear elastic deformations in the breast. These deformations are visualized on breast geometry embedded in an infinite medium with varying ε values in Fig. 1.

$$\mathbb{F}_\varepsilon^{ij}(\boldsymbol{x}) = \boldsymbol{g}_i \cdot \nabla \boldsymbol{f_j}\left[\frac{15\varepsilon^4}{8\pi}\frac{1}{r_\varepsilon^7}\right] \tag{6}$$

$$\left[\mathbb{F}_\varepsilon^{ij}\right]_\times(\boldsymbol{x}) = -r \times f\left[\frac{15\varepsilon^4}{8\pi}\frac{1}{r_\varepsilon^7}\right] \tag{7}$$

$$\mathbf{u}_{\boldsymbol{\varepsilon},\mathbf{twist}}(\boldsymbol{r}) = a\left(\frac{1}{r_\varepsilon^3} + \frac{3\varepsilon^2}{2r_\varepsilon^5}\right)r \times f = [\mathbb{K}_{\text{twist}}(\boldsymbol{r})]_\times f \tag{8}$$

2.2 Registration Task

For registration, $\boldsymbol{x_0}$ control point positions for k number of total regularized Kelvinlets "grab" and "twist" functions are distributed in a predetermined configuration. Then, the

$\boldsymbol{f_{grab}}$ and $\boldsymbol{f_{twist}}$ vectors are optimized to solve for a displacement field that minimizes distance error between geometric data inputs.

For a predetermined configuration of regularized Kelvinlet "grab" and "twist" functions centered at different x_0 control point locations, an elastically deformed state can be represented as the summation of all regularized Kelvinlet displacement fields where $\widetilde{\mathbf{u}}(\boldsymbol{x})$ is the superposed displacement vector and $k = k_{grab} + k_{twist}$ in Eq. (9). Equation (9) can be rewritten in matrix form shown in Eq. (10), where α is a concatenated vector of length $3k$ such that $\boldsymbol{\alpha} = [\boldsymbol{f}^1_{\boldsymbol{grab}}, \boldsymbol{f}^2_{\boldsymbol{grab}}, \ldots, \boldsymbol{f}^{\boldsymbol{k}}_{\boldsymbol{twist}}]$.

$$\widetilde{\mathbf{u}}(x) = \sum_{i=1}^{k_{grab}} \mathbf{u}^{\mathbf{i}}_{\boldsymbol{\varepsilon},\mathbf{grab}}(\boldsymbol{x}) + \sum_{i=1}^{k_{twist}} \mathbf{u}^{\mathbf{i}}_{\boldsymbol{\varepsilon},\mathbf{twist}}(x) \tag{9}$$

$$\widetilde{\mathbf{u}}(x) = \widetilde{\mathbb{K}}(x)\alpha \tag{10}$$

This formulation decouples the forcing magnitudes from the Kelvinlet response matrix $\widetilde{\mathbb{K}}(\boldsymbol{x})$, which is composed of column $\mathbf{u}_{\boldsymbol{\varepsilon},\mathbf{grab}}(\boldsymbol{x})$ and $\mathbf{u}_{\boldsymbol{\varepsilon},\mathbf{twist}}(\boldsymbol{x})$ vectors calculated with unit forcing vectors for each $\mathbb{K}_{\text{grab}}(\boldsymbol{x})$ and $\mathbb{K}_{\text{twist}}(\boldsymbol{x})$ function. This allows for linear scaling of $\widetilde{\mathbb{K}}(\boldsymbol{x})$ using $\boldsymbol{\alpha}$. By setting $\boldsymbol{x_0}$ locations, ε_{grab}, and ε_{twist} as hyperparameters, deformation states can be represented by various $\boldsymbol{\alpha}$ vectors with the registration task being to solve for the optimal $\boldsymbol{\alpha}$ vector.

An objective function is formulated to minimize misalignment between the moving space $\boldsymbol{x_{moving}}$ and fixed space $\boldsymbol{x_{fixed}}$ through geometric data constraints. For the breast imaging datasets in this work, we used simulated intraoperative data features that realistically could be collected in a surgical environment visualized in Fig. 2. The first data feature is MR-visible skin fiducial points placed on the breast surface (Fig. 2, red). These fiducials have known point correspondence. The other two data features are an intra-fiducial point cloud of the skin surface (Fig. 2, light blue) and sparse contour samples of the chest wall surface (Fig. 2, yellow). These data features are surfaces that do not have known correspondence. These data feature designations are consistent with implementations in previous work [16, 17].

For a given deformation state, each data feature contributes to the total error measure. For the point data, the error e^i_{point} for each point i is simply the distance magnitude between corresponding points in $\boldsymbol{x_{fixed}}$ and $\boldsymbol{x_{moving}}$ space. For the surface data, the error $e^i_{surface}$ is calculated as the distance from every point i in the $\boldsymbol{x_{fixed}}$ point cloud surface to the closest point in the $\boldsymbol{x_{moving}}$ surface, projected onto the surface unit normal which allows for sliding contact between surfaces.

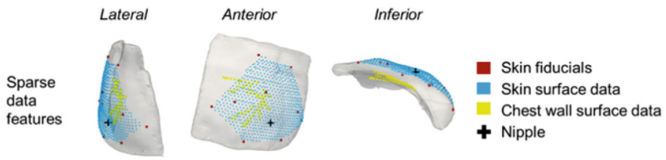

Fig. 2. Sparse data features on breast geometry in the $\boldsymbol{x_{fixed}}$ space.

The optimization using the objective function in Eq. (11) includes two additions to improve the solution. The first is rigid parameters, translation $\boldsymbol{\tau}$ and rotation $\boldsymbol{\theta}$, that are optimized simultaneously with the vector $\boldsymbol{\alpha}$. $\boldsymbol{\beta}$ represents the deformation state with $\boldsymbol{\beta} = [\boldsymbol{\alpha}, \boldsymbol{\tau}, \boldsymbol{\theta}]$, and this compensates for rigid deformation between $\boldsymbol{x_{fixed}}$ and $\boldsymbol{x_{moving}}$. The second is a strain energy regularization term e_{SE} which penalizes deformations with large strain energy. e_{SE} is the average strain energy density within the breast geometry, and it is computed for each $\boldsymbol{\beta}$ at every iteration. It is scaled by weight w_{SE}. The optimal state $\boldsymbol{\beta}$ is iteratively solved using Levenberg-Marquardt optimization terminating at $|\Delta\Omega(\boldsymbol{\beta})| < 10^{-12}$.

$$\Omega(\beta) = \frac{1}{n_{point}} \sum_{i=1}^{n_{point}} \left(e^i_{point}\right)^2 + \frac{1}{n_{surface}} \sum_{i=1}^{n_{surface}} \left(e^i_{surface}\right)^2 + w_{SE}(e_{SE})^2 \tag{11}$$

3 Experiments and Results

In this section, two experiments are conducted. The first explores sensitivity to regularized Kelvinlet function hyperparameters k_{grab}, k_{twist}, ε_{grab}, and ε_{twist} and establishes optimal hyperparameters in a training dataset of 11 breast deformations. The second validates the registration method in a breast cancer patient and compares registration accuracy and computation time to previously proposed methods.

3.1 Hyperparameters Sensitivity Analysis

This dataset consists of supine breast MR images simulating surgical deformations of 11 breasts from 7 healthy volunteers. Volunteers (ages 23–57) were enrolled in a study approved by the Institutional Review Board at Vanderbilt University. Prior to imaging, 26 skin fiducials were distributed on the breast surface. MR images ($0.391 \times 0.391 \times 1$ mm^3 or $0.357 \times 0.357 \times 1$ mm^3) were acquired with the volunteers' arms placed by their sides. This image was used as the $\boldsymbol{x_{moving}}$ space. The volunteers were then instructed to raise one arm above their heads, causing deformation of the ipsilateral breast. A second MR image in the deformed state was acquired to create simulated intraoperative physical data and to use for validation. This second image was used as the $\boldsymbol{x_{fixed}}$ space.

The breast in $\boldsymbol{x_{moving}}$ was segmented at the boundary between the chest wall and breast parenchyma to create a 3D model. The posterior surface was labeled to inform $\boldsymbol{x_0}$ control point locations. The skin fiducials and intra-fiducial surface point clouds were labeled in both images as data features. Sparse tracked ultrasound data collection patterns were projected on the posterior surface for use as the third data feature. Subsurface anatomical targets were labeled in both images and used to compute target error after registration.

Three configurations were explored to test different distributions of grab and/or twist regularized Kelvinlet functions: grab functions only, twist functions only, and a combination of grab and twist functions. Grab function control points were distributed evenly on the posterior surface of the breast to approximate forces from the chest wall. Twist function control points were distributed evenly within the breast to approximate internal body forces. Three hyperparameter sweeps were used:

- Configuration 1: $k_{grab} = \{10, 40, 70, 100\}$, $\varepsilon_{grab} = \{0.005, 0.05, 0.5\}$
- Configuration 2: $k_{twist} = \{10, 40, 70, 100\}$, $\varepsilon_{twist} = \{0.05, 0.1, 0.2\}$
- Configuration 3: $k_{grab} = 40$, $\varepsilon_{grab} = 0.05$, $k_{twist} = \{1, 5, 10, 20\}$, $\varepsilon_{twist} = \{0.05, 0.1, 0.2\}$

For all registrations, mechanical breast properties were set at $\nu = 0.45$, $E = 2100$ Pa, and $w_E = 10^{-9}$ Pa^{-2} [16, 18]. Accuracy was evaluated by measuring target error (distance magnitude between targets in $\boldsymbol{x}_{\boldsymbol{fixed}}$ and registered $\boldsymbol{x}_{\boldsymbol{moving}}$ spaces) for all targets in 11 breast imaging sets totaling 237 targets per registration.

Target error results from hyperparameter sweep registrations are shown in Fig. 3. The registration with the lowest root mean squared error was from configuration 3 $k_{grab} = 40$, $\varepsilon_{grab} = 0.05$, $k_{twist} = 1$, $\varepsilon_{twist} = 0.1$. These hyperparameters were used on a different dataset for validating and comparing the registration method in Sect. 3.2.

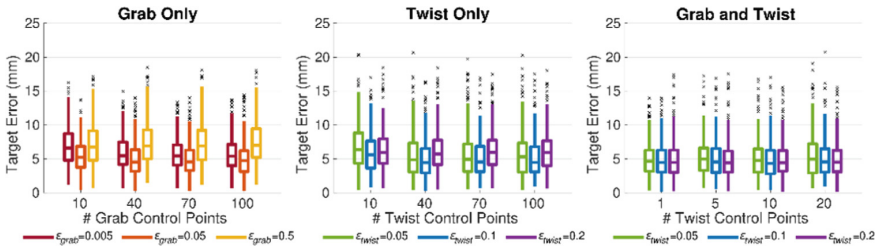

Fig. 3. Target error results from regularized Kelvinlet functions hyperparameter sweeps. Outliers are noted as (x) and are 1.5•IQR.

3.2 Registration Methods Comparison

This dataset consists of supine breast MR images simulating surgical deformations from one breast cancer patient. A 71-year-old patient with invasive mammary carcinoma in the left breast was enrolled in a study approved by the Institutional Review Board at Vanderbilt University. Skin fiducial placement, image acquisition, arm placement, and preprocessing steps followed the same protocol detailed in Sect. 3.1. The tumor was segmented in both images by a subject matter expert, and a 3D tumor model was created to evaluate tumor overlap metrics after registration.

Regularized Kelvinlet function registration was compared to 3 other registration methods: rigid registration, an FEM-based image-to-physical registration method, and an image-to-image registration method. A point-based rigid registration using the skin fiducials provided a baseline comparator for accuracy without deformable correction. The FEM-based image-to-physical registration method, detailed in [12] and implemented in breast in [16], utilizes the same optimization scheme as this method but with an FEM-generated basis. $k = 40$ control points were used for the FEM-based registration. The image-to-image registration method was a symmetric diffeomorphic method with explicit B-spline regularization publicly available in the Advanced Normalization Toolkit (ANTs) repository [19, 20]. Image-to-image registration would not be possible for intraoperative registration in most surgical settings. However, it was included to

demonstrate accuracy when volumetric imaging data is available, as opposed to sparse geometric point data as in the surgical application case. The rigid and image-to-physical registrations were performed on a single thread of a 3.6 GHz AMD Ryzen 7 3700X CPU. Image-to-image registration was multithreaded on 2.3 GHz Intel Xeon (E5–4610 v2) CPUs.

Registration results for the 4 methods are shown in Table 1. The regularized Kelvinlet method accuracy was comparable (if not slightly improved) to the FEM-based method for this example case. Runtime for the regularized Kelvinlet method was improved compared to the FEM-based method. As expected, registration without deformable correction was poor, and image-to-image registration had the best accuracy. Registered tumor geometry results are shown in Fig. 4.

Table 1. Registration performance for 4 methods. HD – Hausdorff distance.

		Rigid	Image-to-Physical		Image-to-Image
			FEM	R. Kelvinlets	
Point metrics	Fiducial Error (mm)	7.4 ± 2.0	0.7 ± 0.5	1.4 ± 0.6	2.0 ± 1.7
	Target Error (mm)	6.1 ± 1.4	3.3 ± 1.1	3.0 ± 1.1	2.3 ± 1.5
Tumor overlap metrics	Dice Coefficient	2.3%	32.7%	49.5%	85.8%
	Centroid Distance (mm)	7.3	4.4	3.5	1.3
	Modified HD (mm)	4.1	2.2	1.7	0.6
Runtime (seconds)		< 1	188	14	15,942

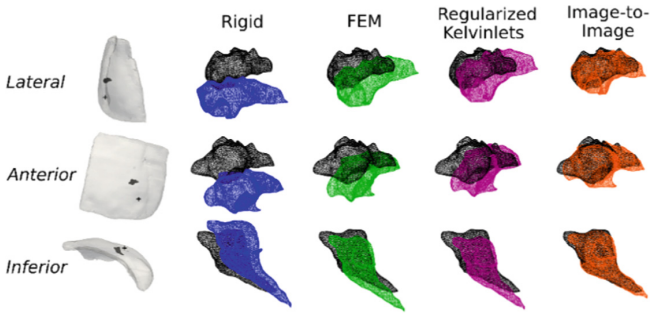

Fig. 4. Tumor overlap after registration. Black – $\boldsymbol{x}_{\boldsymbol{fixed}}$ tumor used for validation. Blue – rigidly registered $\boldsymbol{x}_{\boldsymbol{moving}}$ tumor. Green – FEM-based registered $\boldsymbol{x}_{\boldsymbol{moving}}$ tumor. Pink – regularized Kelvinlet function registered $\boldsymbol{x}_{\boldsymbol{moving}}$ tumor. Orange – image-to-image registered $\boldsymbol{x}_{\boldsymbol{moving}}$ tumor.

4 Limitations and Conclusion

Several limitations should be noted. Regularized Kelvinlet functions describe solutions that assume a physical embedding within an infinite elastic domain, which does not account for organ-specific geometry. This approach may not be well suited for problems where geometry has significant influence. This method is derived from a linear elastic model, and nonlinear models are known to better describe soft tissue mechanics. Additionally, this method assumes homogeneity and isotropy – it does not account for different tissue types and directional structures in the breast. With regards to clinical feasibility, supine MR imaging with skin fiducials is not the standard-of-care. However, using supine MR imaging for surgery is becoming increasingly investigated, and previous work demonstrated the potential of ink-based skin fiducial markings on the breast [21, 22]. Despite these limitations, this method's accuracy and speed may be appropriate for surgical guidance applications.

In this work, we demonstrated the use of regularized Kelvinlet functions for image-to-physical registration of the breast. We achieved near real-time registration with comparable accuracy to previously proposed methods. We believe that this approach is generalizable to other soft-tissue organ systems and is well-suited for improving navigation during image-guided surgeries.

Acknowledgements. This work was supported by the National Institutes of Health through Grant Nos. R01EB027498 and T32EB021937, the National Science Foundation for a Graduate Research Fellowship awarded to M.R., and the Vanderbilt Center for Human Imaging supported by Grant No. 1S10OD021771-01 for the 3T MRI.

References

1. Alam, F., Rahman, S.U., Ullah, S., Gulati, K.: Medical image registration in image guided surgery: Issues, challenges and research opportunities. Biocybern. Biomed. Eng. **38**, 71–89 (2018)
2. Gavriilidis, P., et al.: Navigated liver surgery: state of the art and future perspectives. Hepatob. Pancreat. Dis. Int. **21**, 226–233 (2022)
3. Schmidt, F.A., et al.: Elastic image fusion software to coregister preoperatively planned pedicle screws with intraoperative computed tomography data for image-guided spinal surgery. Int. J. Spine Surg. **15**, 295–301 (2021)
4. Collins, J.A., et al.: Improving registration robustness for image-guided liver surgery in a novel human-to-phantom data framework HHS public access. IEEE Trans. Med. Imaging. **36**, 1502–1510 (2017)
5. Conley, R.H., et al.: Realization of a biomechanical model-assisted image guidance system for breast cancer surgery using supine MRI. Int. J. Comput. Assist. Radiol. Surg. **10**, 1985 (2015)
6. Zettinig, O., et al.: Multimodal image-guided prostate fusion biopsy based on automatic deformable registration. Int. J. Comput. Assist. Radiol. Surg. **10**(12), 1997–2007 (2015). https://doi.org/10.1007/s11548-015-1233-y
7. Kaczmarski, K., et al.: Surgeon re-excision rates after breast-conserving surgery: a measure of low-value care. J. Am. Coll. Surg. **228**, 504-512.e2 (2019)

8. Pfeiffer, M., et al.: Non-rigid volume to surface registration using a data-driven biomechanical model. In: Martel, A.L., et al. (eds.) Medical Image Computing and Computer Assisted Intervention – MICCAI 2020. LNCS, vol. 12264, pp. 724–734. Springer, Cham (2020). https://doi.org/10.1007/978-3-030-59719-1_70
9. Fu, Y., et al.: Biomechanically constrained non-rigid MR-TRUS prostate registration using deep learning based 3D point cloud matching. Med. Image Anal. **67**, 101845 (2021)
10. Balakrishnan, G., Zhao, A., Sabuncu, M.R., Guttag, J., Dalca, A.V.: VoxelMorph: a learning framework for deformable medical image registration. IEEE Trans. Med. Imaging **38**(8), 1788–1800 (2019). https://doi.org/10.1109/TMI.2019.2897538
11. Peterlík, I., et al.: Fast elastic registration of soft tissues under large deformations. Med. Image Anal. **45**, 24–40 (2018)
12. Heiselman, J.S., Jarnagin, W.R., Miga, M.I.: Intraoperative correction of liver deformation using sparse surface and vascular features via linearized iterative boundary reconstruction. IEEE Trans. Med. Imaging. **39**, 2223–2234 (2020)
13. Belytschko, T., Lu, Y.Y., Gu, L.: Element-free Galerkin methods. Int. J. Numer. Methods Eng. **37**, 229–256 (1994)
14. Zhang, L.W., Ademiloye, A.S., Liew, K.M.: Meshfree and particle methods in biomechanics: prospects and challenges. Arch. Comput. Methods Eng. **26**(5), 1547–1576 (2018). https://doi.org/10.1007/s11831-018-9283-2
15. De Goes, F., James, D.L.: Regularized kelvinlets: sculpting brushes based on fundamental solutions of elasticity. ACM Trans. Graph. **36**(4), 1–11 (2017). https://doi.org/10.1145/3072959.3073595
16. Richey, W.L., Heiselman, J.S., Ringel, M.J., Meszoely, I.M., Miga, M.I.: Computational imaging to compensate for soft-tissue deformations in image-guided breast conserving surgery. IEEE Trans. Biomed. Eng. **69**, 3760–3771 (2022)
17. Richey, W.L., Heiselman, J.S., Ringel, M.J., Meszoely, I.M., Miga, M.I.: Tumor deformation correction for an image guidance system in breast conserving surgery. In: SPIE Proceedings, 12034 (2022)
18. Griesenauer, R.H., Weis, J.A., Arlinghaus, L.R., Meszoely, I.M., Miga, M.I.: Breast tissue stiffness estimation for surgical guidance using gravity-induced excitation. Phys. Med. Biol. **62**, 4756–4776 (2017)
19. Tustison, N.J., Avants, B.B.: Explicit B-spline regularization in diffeomorphic image registration. Front. Neuroinform. **7**, 39 (2013)
20. Ringel, M.J., Richey, W.L., Heiselman, J.S., Luo, M., Meszoely, I.M., Miga, M.I.: Supine magnetic resonance image registration for breast surgery: insights on material mechanics. J. Med. Imaging. **9**, 065001 (2022)
21. Gombos, E.C., et al.: Intraoperative supine breast MR imaging to quantify tumor deformation and detection of residual breast cancer: preliminary results. Radiology **281**, 720–729 (2016)
22. Richey, W.L., Heiselman, J.S., Ringel, M.J., Ingrid, M., Meszoely, M.I., Miga, M.I.: Soft tissue monitoring of the surgical field: detection and tracking of breast surface deformations. IEEE Trans. Biomed. Eng. **70**(7), 2002–2012 (2023). https://doi.org/10.1109/TBME.2022.3233909